Nonlinear thermal radiation and magnetic field effects on the flow Carreau nanofluid with convective conditions

Sajid Qayyum [a], Tasawar Hayat [a,b], Ahmed Alsaedi [b] and Bashir Ahmad [b]

[a] Department of Mathematics, Quaid-I-Azam University 45320, Islamabad 44000, Pakistan

[b] Nonlinear Analysis and Applied Mathematics (NAAM) Research Group, Faculty of Science, King Abdulaziz University P. O. Box 80207, Jeddah 21589, Saudi Arabia

[*]Corresponding author: sajidqayyum94@gmail.com (Sajid Qayyum)

Abstract: Main features of the present analysis is to investigate the magnetohydrodynamic (MHD) nonlinear mixed convection flow of Carreau nanofluid. Flow is due to stretching sheet with thermal and solutal convective conditions. Intention in present analysis is to develop a model for nanomaterial. The nonlinear ordinary differential systems are obtained. Homotopy algorithm leads to solutions development. Velocity, temperature, nanoparticles concentration, surface drag force and heat and mass transfer rate are displayed and argued. It is revealed that qualitative behaviors of velocity and layer thickness are reverse for material and magnetic parameters. Temperature field and heat transfer rate are similar observation for thermal Biot numbers. Moreover qualitative behaviors of nanoparticles concentration and mass transfer rate are reverse for larger Brownian motion.

Keywords: Carreau nanofluid; magnetohydrodynamic (MHD); nonlinear convection; nonlinear thermal radiation; convective conditions.

1 Introduction

There are various fluids of industrial and engineering importance such as petroleum production, multigrade oils, polymers, composite material, shampoos and fruit juices that show the viscoelastic aspects. Such fluids cannot be characterized simply like the Newtonian fluids. Because of the diversity of flow in nature, various non-Newtonian models have been recommended by the investigators [1, 2]. Among these models, Carreau fluid is one having importance in chemical engineering. Bird et al. [3] explained the detail of Carreau materials which are generally recognized as generalized Newtonian fluids. This model fits the performance of suspension of polymers in numerous fluid problems. It shows the viscous fluid purely where viscosity varies due to deformation rate. Ali and Hayat [4] discussed peristalsis of Carreau liquid

in an asymmetric channel. Hayat et al. [5] analyzed the aspects of heat transfer in flow of Carreau fluid towards a stretched sheet. Hayat et al. [6] studied nonlinear convective flow of Carreau nanofluid in the presence of Brownian motion and thermophoresis aspects. Hsiao [7] inspected MHD stagnation point flow of a Carreau nanoliquid towards a stretching surface. Features of Newtonian heating and MHD flow of Carreau liquid presented by Hayat et al. [8]. MHD flow of Carreau nanofluid with mass flux condition is investigated by Khan et al. [9]. Khan et al. [10] studied the radiative flow of Carreau nanofluid with heat generation/absorption.

The features of nonlinear thermal radiation in boundary layer flow is significant due to its application in industrial and engineering fields such as, furnace design, glass production, polymer processing, gas cooled nuclear reactors and also in space technology like aerodynamics rockets, propulsion system, missiles, power plants for inter planetary flights and space crafts which works at high temperatures. Consequently, thermal radiation effects cannot be ignored in such processes. The radiative heat flux in the energy equation is described through Rosseland relation. Cortell [11] examined the features of nonlinear radiative flow of viscous fluid in the frame of stretched sheet. Hayat et al. [12] studied the mixed convection flow of tangent hyperbolic nanofluid with nonlinear thermal radiation. An analysis for methanol and kerosene based ferrofluids flow with nonlinear radiation is established by Reddy et al. [13]. Characteristics of nonlinear thermal radiation and magnetic field flow of Sisko nanofluid has been studied by Soomro et al. [14]. Laxmi and Shankar [15] analyzed the radiative flow of viscous fluid in the frame of injection/suction. Some prominent literature for nonlinear thermal radiation can be studied in the refs. [16-20].

Recent work has shown evidence that nanofluids are likely to have better thermal efficiency through the base fluids. Such fluids can be used in the procedures of vehicle computers, nuclear reactors, electronic cooling equipment, transportation and transformer cooling, heating and cooling process of energy conversion, cancer therapy etc. Choi [21] provided an experimental work on nanofluid in view of various mechanisms. He concluded that the nanofluid is best suitable candidate for the betterment in heat transfer of ordinary liquids. Buongiorno [22] presented a detailed discussion on the effectiveness of nanoparticles in convective transport of ordinary fluids. Significance of CuO-water nanoparticles on surface of heat exchangers has been experimentally addressed by Pantzali et al. [23]. Hamad et al. [24] explain the laminar flow of

viscous nanofluid in the frame of porous medium. Magnetohydrodynamic flow of tangent-hyperbolic nanofluid towards a stretching sheet has been reported by Hayat et al. [25]. Stagnation point flow of Jeffrey nanofluid with magnetic field has been investigated by Chakraborty [26]. Further relevant studies involving nanofluids can be seen through the investigations [27-30] and various studies therein.

The results obtained by homotopy analysis method (HAM) are preferred than the numerical solutions in perspective of the following points [31-40]. (a) HAM gives the solutions within the domain of interest at each point while the numerical solutions hold just for discrete points in the domain. (b) Algebraically developed approximate solutions require less effort and having a sensible measure of precision when compared to numerical solution which are more convenient for the scientist, an engineer or an applied mathematician. (c) Although most of the scientific packages required some initial approximations for the solution are not generally convergent. In such conditions approximate solutions can offer better initial guess that can be readily advanced to the exact numerical solution in the limited iterations. Finally an approximate solution, if it is analytical, is most pleasing than the numerical solutions.

Here our main emphasize is to visualize the nonlinear mixed convection flow of Carreau nanofluid generated by movement of radiative sheet. Nonlinear radiation term is incorporated in energy expression. Solutal and thermal convective conditions are considered. Aspects of magnetohydrodynamic are analyzed in the mathematical modelling. The velocity, thermal field, nanoparticle concentration, surface drag force and heat and mass transfer rate are graphically sketched and analyzed for various physical parameters.

2 Mathematical description

Let us investigate two dimensional nonlinear mixed convection flow of Carreau nanofluid past a stretched sheet at $y = 0$. Flow restricted is in the domain $y > 0$. Stretching surface has velocity $u_w(x) = ax$ (where a is the dimensional constant). A magnetic field of strength B_0 is parallel in the $y-$direction. Induced magnetic field is absent for small magnetic Reynolds number. Nonlinear thermal radiation, Brownian motion and thermophoresis aspects are retained. Solutal and thermal convective conditions are imposed. Flow equations of Carreau nanofluid subject to usual boundary layer approximations give

$$\frac{\partial u}{\partial x}+\frac{\partial v}{\partial y}=0, \tag{1}$$

$$\begin{aligned} u\frac{\partial u}{\partial x}+v\frac{\partial u}{\partial y}=\nu\frac{\partial^2 u}{\partial y^2}\left[1+\left(\frac{n-1}{2}\right)\lambda^{*2}\left(\frac{\partial u}{\partial y}\right)^2\right]-\frac{\sigma B_0^2}{\rho}u \\ +\nu(n-1)\lambda^{*2}\left[\frac{\partial^2 u}{\partial y^2}\left(\frac{\partial u}{\partial y}\right)^2\right]\left[1+\left(\frac{n-3}{2}\right)\lambda^{*2}\left(\frac{\partial u}{\partial y}\right)^2\right] \\ +g\{\Lambda_1(T-T_\infty)+\Lambda_2(T-T_\infty)^2\}+g\{\Lambda_3(C-C_\infty)+\Lambda_4(C-C_\infty)^2\}, \end{aligned} \tag{2}$$

$$u\frac{\partial T}{\partial x}+v\frac{\partial T}{\partial y}=\frac{k_f}{(\rho c_p)_f}\left(\frac{\partial^2 T}{\partial y^2}\right)+\tau D_B\left(\frac{\partial T}{\partial y}\frac{\partial C}{\partial y}\right)+\frac{\tau D_T}{T_\infty}\left(\frac{\partial T}{\partial y}\right)^2-\frac{1}{(\rho c_p)_f}\frac{\partial q_r}{\partial y}, \tag{3}$$

$$u\frac{\partial C}{\partial x}+v\frac{\partial C}{\partial y}=D_B\left(\frac{\partial^2 C}{\partial y^2}\right)+\frac{D_T}{T_\infty}\left(\frac{\partial^2 T}{\partial y^2}\right), \tag{4}$$

with related boundary conditions are

$$\begin{aligned} &u=u_w(x)=ax,\ \ v=0,\ \ -k\frac{\partial T}{\partial y}=h_t(T_f-T),\ \ -D_B\frac{\partial C}{\partial y}=h_c(C_f-C)\ \text{ at }\ y=0, \\ &u\to 0,\ \ T\to T_\infty,\ \ C\to C_\infty\ \text{ as }\ y\to\infty, \end{aligned} \tag{5}$$

where u and v are velocity components corresponding to x and y directions respectively, $\nu=(\mu/\rho)_f$ for kinematic viscosity, λ^* for time constant, σ for electrical conductivity, Λ_1 and Λ_2 for linear and nonlinear thermal expansions coefficients, Λ_3 and Λ_4 for linear and nonlinear concentration expansion coefficients, ρ_f and ρ_p for fluid and particle densities, $(c_p)_f$ and $(c_p)_p$ for fluid and particle heat capacities, k_f for thermal conductivity, q_r for radiative heat flux, $\tau=(\rho c_p)_p/(\rho c_p)_f$ for capacity ratio, D_B and D_T for Brownian and themophoresis diffusion coefficients, T and C for fluid temperature and concentration, T_∞ and C_∞ for ambient fluid temperature and nanoparticle concentration, n for power law index, h_t and h_c for coefficient of heat and mass transfer.

By Rosseland approximation, radiative heat flux q_r is

$$q_r = -\frac{4\sigma^*}{3k^*}\frac{\partial T^4}{\partial y} = -\frac{16\sigma^*}{3k^*}T^3\frac{\partial T}{\partial y}, \tag{6}$$

where σ^* and k^* present the Stefan-Boltzmann constant and the Rosseland mean absorption coefficient respectively. Now Eqs. (3) and (6) yield

$$\begin{aligned} u\frac{\partial T}{\partial x} + v\frac{\partial T}{\partial y} = \frac{k_f}{\left(\rho c_p\right)_f}\frac{\partial^2 T}{\partial y^2} + \tau D_B\left(\frac{\partial T}{\partial y}\frac{\partial C}{\partial y}\right) + \frac{\tau D_T}{T_\infty}\left(\frac{\partial T}{\partial y}\right)^2 \\ + \frac{1}{\left(\rho c_p\right)_f}\frac{16\sigma^*}{3k^*}\frac{\partial}{\partial y}\left(T^3\frac{\partial T}{\partial y}\right). \end{aligned} \tag{7}$$

By using the similarity variables

$$\begin{aligned} &\eta = \sqrt{\frac{a}{\nu}}y,\ \theta(\eta) = \frac{T - T_\infty}{T_f - T_\infty} \text{ or } T = T_\infty(1 + (\theta_w - 1)\theta),\ \phi(\eta) = \frac{C - C_\infty}{C_f - C_\infty}, \\ &u = axf'(\eta),\ v = -\sqrt{a\nu}\,f(\eta),\ \psi(\eta) = \sqrt{a\nu}\,xf(\eta). \end{aligned} \tag{8}$$

Eq. (1) is trivially satisfied and other equations yield

$$\begin{aligned} &f'''\left(1 + \left(\frac{n-1}{2}\right)\alpha f''^2\right) + 2\left[\left(\frac{n-1}{2}\right)\alpha f''^2\right]\left[1 + \left(\frac{n-3}{2}\right)\alpha f''^2\right] \\ &+ ff'' - f'^2 - H_a^2 f' + \lambda(1 + \beta_t\theta)\theta + \lambda N^*(1 + \beta_c\phi)\phi = 0, \end{aligned} \tag{9}$$

$$\begin{aligned} &\left(1 + \frac{4}{3}R\right)\theta'' + \frac{4}{3}R\left[(\theta_w - 1)^3\left(3\theta^2(\theta')^2 + \theta^3\theta''\right) + 3(\theta_w - 1)^2\left(2\theta(\theta')^2 + \theta^2\theta''\right)\right. \\ &\left. + 3(\theta_w - 1)\left((\theta')^2 + \theta\theta''\right)\right] + \Pr\, f\theta' + \Pr\, N_b\theta'\phi' + \Pr\, N_t(\theta')^2 = 0, \end{aligned} \tag{10}$$

$$\phi'' + Scf\phi' + \frac{N_t}{N_b}\theta'' = 0, \tag{11}$$

$$\begin{aligned} &f'(\eta) = 1,\ f(\eta) = 0,\ \theta'(\eta) = -B_t(1 + \theta(\eta)),\ \phi'(\eta) = -B_c(1 + \phi(\eta)) \text{ at } \eta = 0, \\ &f'(\eta) = 0,\ \theta(\eta) = 0,\ \phi(\eta) = 0 \text{ as } \eta \to \infty, \end{aligned} \tag{12}$$

where α for material variable, H_a for magnetic parameter/Hartman number, λ for mixed convection variable, β_t and β_c for nonlinear convection variable due to temperature and

concentration, N^* for concentration to thermal buoyancy forces ratio, R for radiation parameter, θ_w for temperature variable, Pr for Prandtl number, N_b for Brownian motion variable, N_t for thermophoresis variable, Sc for Schmidt number, Gr and Gr^* for Grashof number in terms of temperature and concentration and B_t and B_c for Biot numbers in view of heat and mass transfer. Definitions of these variables are

$$\begin{aligned}
&\alpha=\lambda^{*2}a^2,\ H_a=\frac{\sigma B_0^2}{\rho a},\ \lambda=\frac{Gr}{\mathrm{Re}_x^2},\ \beta_t=\frac{\Lambda_2(T_f-T_\infty)}{\Lambda_1},\ N^*=\frac{Gr^*}{Gr}=\frac{\Lambda_3\left(C_f-C_\infty\right)}{\Lambda_1\left(T_f-T_\infty\right)},\\
&\beta_c=\frac{\Lambda_4\left(C_f-C_\infty\right)}{\Lambda_3},\ R=\frac{4\sigma^*T_\infty^3}{k_f k^*},\ \theta_w=\frac{T_f}{T_\infty},\ \mathrm{Pr}=\frac{\mu c_p}{k_f},\ N_b=\frac{\tau D_B\left(C_f-C_\infty\right)}{\nu},\\
&N_t=\frac{\tau D_T\left(T_f-T_\infty\right)}{\nu T_\infty},\ Sc=\frac{\nu}{D_B},\ B_t=\frac{h_t}{k}\sqrt{\frac{\nu}{a}},\ B_c=\frac{h_c}{D_B}\sqrt{\frac{\nu}{a}},\ Gr=\frac{g\Lambda_1\left(T_f-T_\infty\right)x^3}{\nu^2},\\
&Gr^*=\frac{g\Lambda_3(C_f-C_\infty)x^3}{\nu^2}.
\end{aligned}\tag{13}$$

2.1 Physical quantities

The surface drag force $\left(C_{f_x}\right)$, heat transfer rate $\left(Nu_x\right)$ and mass transfer rate $\left(Sh_x\right)$ are interpreted as

$$C_{f_x}=\frac{\tau_w}{\frac{1}{2}\rho u_w^2},\ Nu_x=\frac{xq_w}{k_f(T_f-T_\infty)},\ Sh_x=\frac{xj_w}{D_B(C_f-C_\infty)},\tag{14}$$

in which τ_w, q_w and j_w denote the surface shear stress and the surface heat and mass fluxes respectively. Here are

$$\begin{aligned}
&\tau_w=\eta_0\left[\left(\frac{\partial u}{\partial y}\right)+\lambda^{*2}\left(\frac{n-1}{2}\right)\left\{\frac{\partial u}{\partial y}\left(\frac{\partial u}{\partial x}\right)^2+3\frac{\partial v}{\partial x}\left(\frac{\partial u}{\partial y}\right)^2\right\}\right]_{y=0},\\
&q_w=-k_f\left(1+\frac{4}{3}\frac{4\sigma^*T_\infty^3}{k_f k^*}\right)\left(\frac{\partial T}{\partial y}\right)_{y=0},\ j_w=-D_B\left(\frac{\partial C}{\partial y}\right).
\end{aligned}\tag{15}$$

In dimensionless form these quantities are expressed as

$$\frac{1}{2}\mathrm{Re}_x^{0.5}\,C_{f_x}=\left(1+\alpha\left(\frac{n-1}{2}\right)\right)f''(0),\ \ \mathrm{Re}_x^{-0.5}\,Nu_x=-\left(1+\frac{4}{3}R\left(1+(\theta_w-1)\theta(0)\right)^3\right)\theta'(0),$$
$$\mathrm{Re}_x^{-0.5}\,Sh_x=-\phi'(0), \tag{16}$$

where $\mathrm{Re}_x=\frac{u_w x}{\nu}$ present local Reynolds number.

3 Homotopy analysis solutions

We choose the initial guesses $f_0(\eta)$, $\theta_0(\eta)$ and $\phi_0(\eta)$ and linear operators $\mathbf{L}_f$, $\mathbf{L}_\theta$ and $\mathbf{L}_\phi$ for the velocity, temperature and concentration are expressed in the forms

$$f_0(\eta)=1-\exp(-\eta),\ \theta_0(\eta)=\frac{B_t}{1+B_t}\exp(-\eta),\ \phi_0(\eta)=\frac{B_c}{1+B_c}\exp(-\eta), \tag{17}$$

$$\mathbf{L}_f(f)=\frac{d^3f}{d\eta^3}-\frac{df}{d\eta},\ \ \mathbf{L}_\theta(\theta)=\frac{d^2\theta}{d\eta^2}-\theta,\ \ \mathbf{L}_\phi(\phi)=\frac{d^2\phi}{d\eta^2}-\phi, \tag{18}$$

with the properties

$$\begin{aligned}&\mathbf{L}_f\left[\Gamma_1+\Gamma_2\exp(-\eta)+\Gamma_3\exp(\eta)\right]=0,\\&\mathbf{L}_\theta\left[\Gamma_4\exp(-\eta)+\Gamma_5\exp(\eta)\right]=0,\\&\mathbf{L}_\phi\left[\Gamma_6\exp(-\eta)+\Gamma_7\exp(\eta)\right]=0.\end{aligned} \tag{19}$$

We obtain the general solutions $f_m(\eta)$, $\theta_m(\eta)$ and $\phi_m(\eta)$ through the following procedure of refs. [37-40]:

$$\begin{aligned}f_m(\eta)&=f_m^*(\eta)+\Gamma_1+\Gamma_2\exp(-\eta)+\Gamma_3\exp(\eta),\\\theta_m(\eta)&=\theta_m^*(\eta)+\Gamma_4\exp(-\eta)+\Gamma_5\exp(\eta),\\\phi_m(\eta)&=\phi_m^*(\eta)+\Gamma_6\exp(-\eta)+\Gamma_7\exp(\eta),\end{aligned} \tag{20}$$

in which $f_m^*(\eta)$, $\theta_m^*(\eta)$ and $\phi_m^*(\eta)$ denote the special functions and Γ_i $(i=1-7)$ are the arbitrary constants given by

$$\Gamma_1 = -\left.\frac{\partial f_m^*(\eta)}{\partial \eta}\right|_{\eta=0} - f_m^*(0),\ \Gamma_2 = \left.\frac{\partial f_m^*(\eta)}{\partial \eta}\right|_{\eta=0},\ \Gamma_3 = 0,$$

$$\Gamma_4 = \frac{1}{1+B_t}\left[\left.\frac{\partial \theta_m^*(\eta)}{\partial \eta}\right|_{\eta=0} - B_t\theta_m^*(0)\right],\ \Gamma_5 = 0, \tag{21}$$

$$\Gamma_6 = \frac{1}{1+B_c}\left[\left.\frac{\partial \phi_m^*(\eta)}{\partial \eta}\right|_{\eta=0} - B_c\phi_m^*(0)\right],\ \Gamma_7 = 0.$$

3.1 Convergence of the homotopy solutions

The homotopy analysis method contains auxiliary variables $\hbar_f$, $\hbar_\theta$ and $\hbar_\phi$. These auxiliary variables are efficient in adjusting and controlling the convergence. To obtain valid ranges of these variables, the $\hbar$-curves are sketched at 20^{th}-order of approximations (see Fig. 1). By looking at the range of variables the decisive values of $\hbar_f$, $\hbar_\theta$ and $\hbar_\phi$ are $-1.55 \le \hbar_f \le -0.15$, $-1.60 \le \hbar_\theta \le -0.1$ and $-1.45 \le \hbar_\phi \le -0.15$.

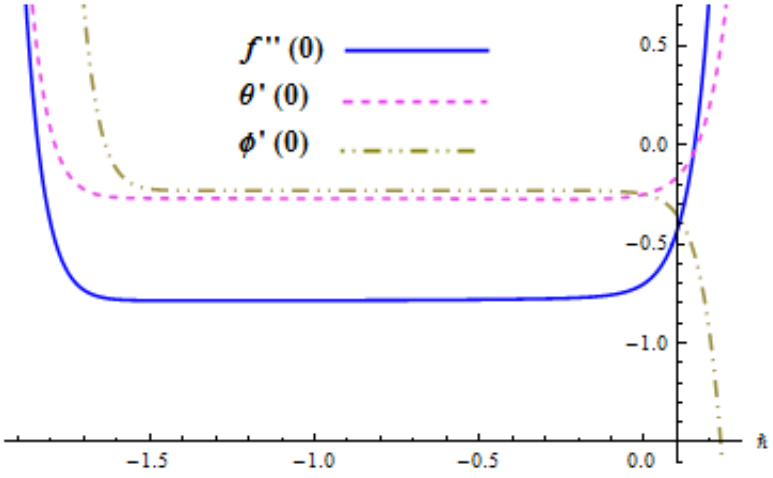

Fig. 1. $\hbar$-curves for $f''(0)$, $\theta'(0)$ and $\phi'(0)$.

Table 1: Convergence solutions when $n = 2.0$, $\alpha = 0.2$, $H_a = 0.1$, $\lambda = 0.1$, $\beta_t = 0.1$, $N^* = 0.5$, $\beta_c = 0.1$, $R = 0.3$, $\theta_w = 1.1$, $\Pr = 2.0$, $N_b = 0.2$, $N_t = 0.1$, $Sc = 2.0$, $B_t = 0.2$ and $B_c = 0.2$.

Order of approximation	$-f''(0)$	$-\theta'(0)$	$-\phi'(0)$
1	0.9513	0.1601	0.1602
5	0.9220	0.1549	0.1556
6	0.9210	0.1548	0.1555
10	0.9197	0.1548	0.1555
15	0.9197	0.1548	0.1555
20	0.9197	0.1548	0.1555
25	0.9197	0.1548	0.1555

Table 1 is analyzed for convergence of the homotopic solutions. Here we observed that convergence for velocity is achieved 10^{th} order of approximations and temperature and nanoparticles concentration is achieved at 6^{th} order of approximations.

4 Graphical results

The features of various physical quantities for velocity, temperature, nanoparticles concentration, surface drag force and heat and mass transfer rate are scrutinized through graphs. The used values of the quantities here are $n = 2.0,\ \alpha = 0.2,\ H_a = 0.1,\ \lambda = 0.1,\ \beta_t = 0.1,\ N^* = 0.5,$ $\beta_c = 0.1,\ R = 0.3,\ \theta_w = 1.1,\ \Pr = 2.0,\ N_b = 0.2,\ N_t = 0.1,\ Sc = 2.0,\ B_t = 0.2$ and $B_c = 0.2.$

4.1 Velocity field

Characteristics of n versus velocity is explored in Fig. 2. Clearly velocity and layer thickness increases when n is enhanced. In fact higher values of n increase nonlinearity of the surface and this helps to reduce the resistive force. Fig. 3 addresses α aspects versus velocity. It is noted that both velocity and layer thickness are increased via α. Explanation of H_a on velocity are described via Fig. 4. Clearly velocity reduces with an increment in H_a. It is because of the reason that Lorentz force acts as a retarding force. Such retarding force enhances the frictional resistance opposing the liquid motion in the momentum boundary layer thickness. Velocity for λ is drawn in Fig. 5. Both velocity and layer thickness are boosted for larger λ. In fact that larger λ give rise to more buoyancy force and so velocity and layer thickness are enhanced.

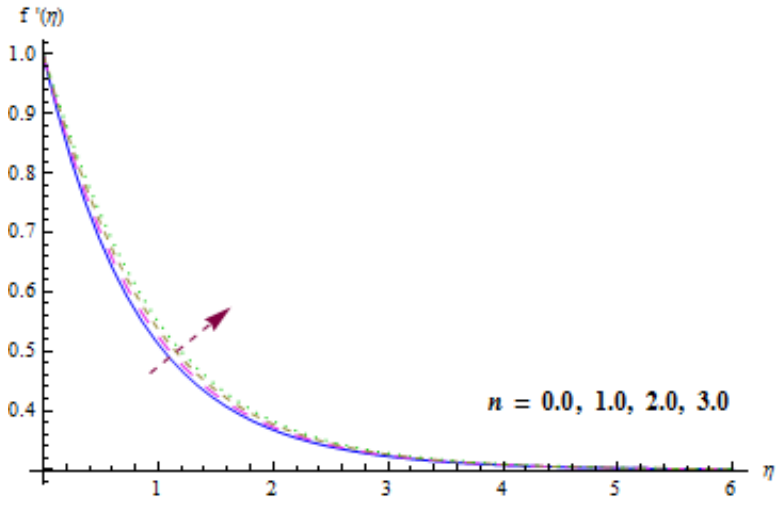

Fig. 2. $f'(\eta)$ via variation of n.

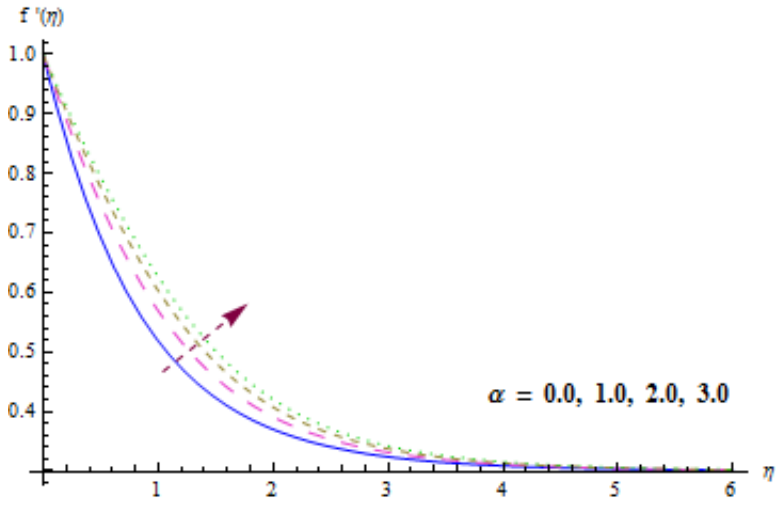

Fig. 3. $f'(\eta)$ via variation of α.

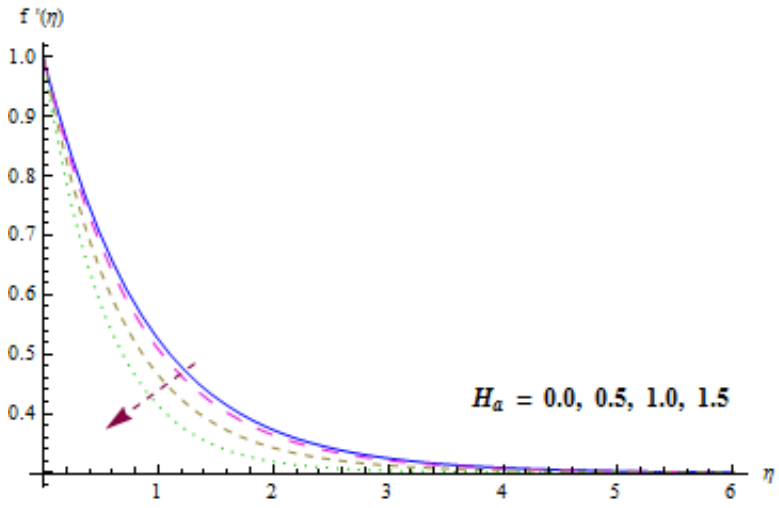

Fig. 4. $f'(\eta)$ via variation of H_a.

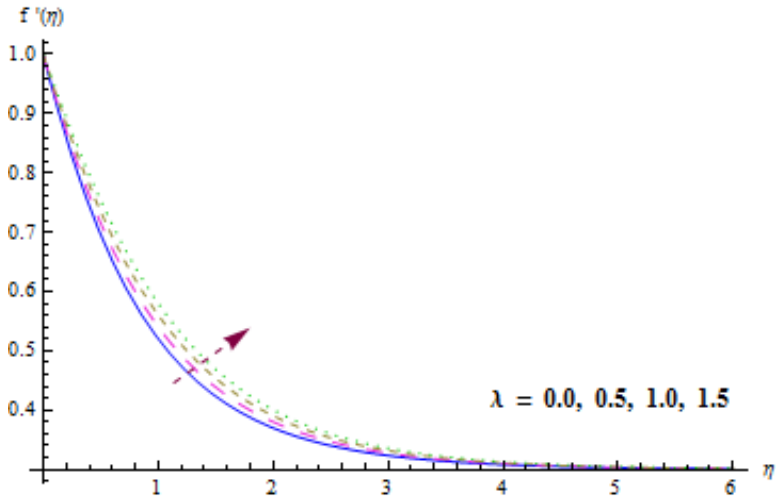

Fig. 5. $f'(\eta)$ via variation of λ.

4.2 Temperature field

Fig. 6 disclosed the behavior of R. Temperate and layer thickness are increasing functions of R. As expected heat is produced due to radiation process in the working fluid so temperature field enhances. Fig. 7 predicts the temperature field for θ_w. Both thermal field and related thickness layer boost when we increase values of θ_w (i.e., temperature variable). Physically higher θ_w lead to an increase in convective surface temperature. Ultimate thermal field increases. Aspect of Pr on temperature is described in Fig. 8. Here both temperature and its layer thickness are reduced

for larger Pr. Physically higher Pr lead to low thermal diffusivity which is responsible for temperature reduction. Fig. 9 emphases temperature variation via N_b. For larger N_b both temperature and layer thickness are increased. In fact more heat is produced through random motion of the fluid particles due to larger Brownian motion variable and consequently the temperature enhances. Temperature versus N_t is disclosed in Fig. 10. It is clear that both temperature and related layer thickness for larger N_t. In thermophoresis phenomenon heated particles are pulled away from hot surface to the cold region. Due to this fact the fluid temperature enhances. Fig. 11 emphases on temperature versus B_t. Obviously temperature and its related layer thickness have increasing function for B_t.

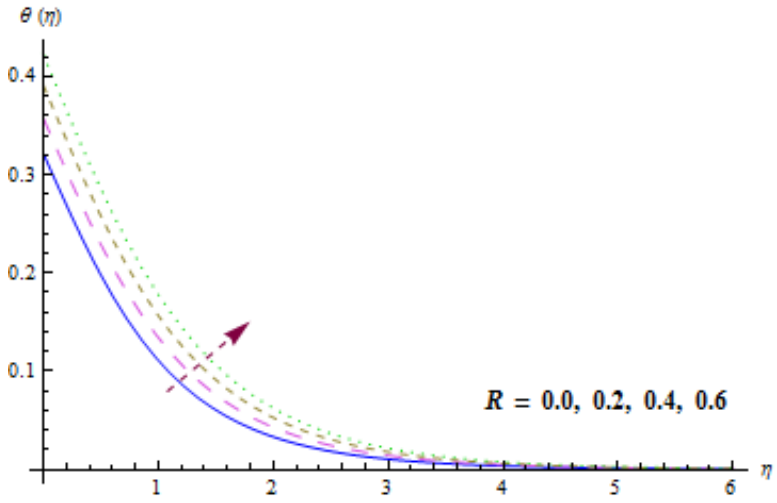

Fig. 6. $\theta(\eta)$ via variation of R.

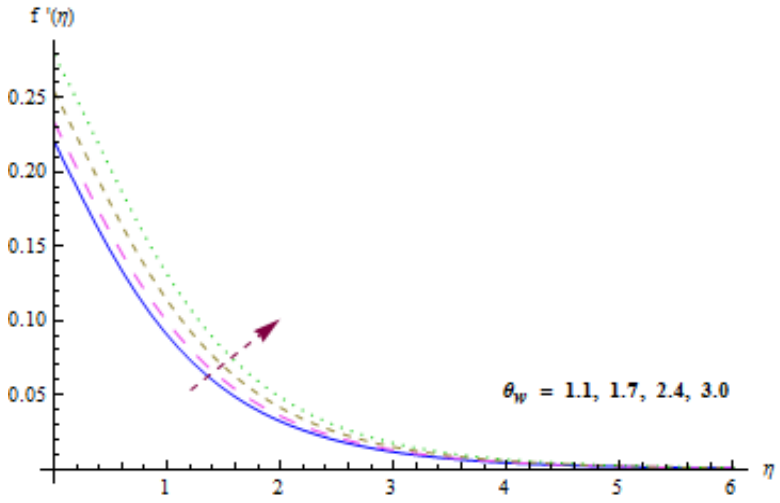

Fig. 7. $\theta(\eta)$ via variation of θ_w.

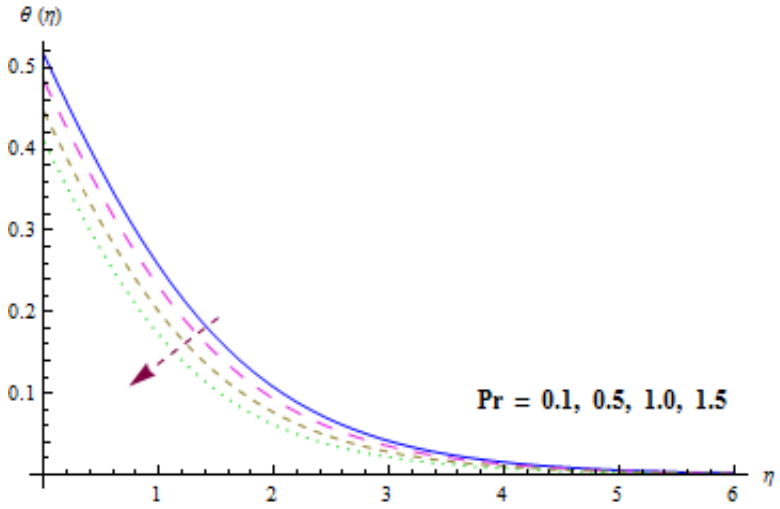

Fig. 8. $\theta(\eta)$ via variation of Pr.

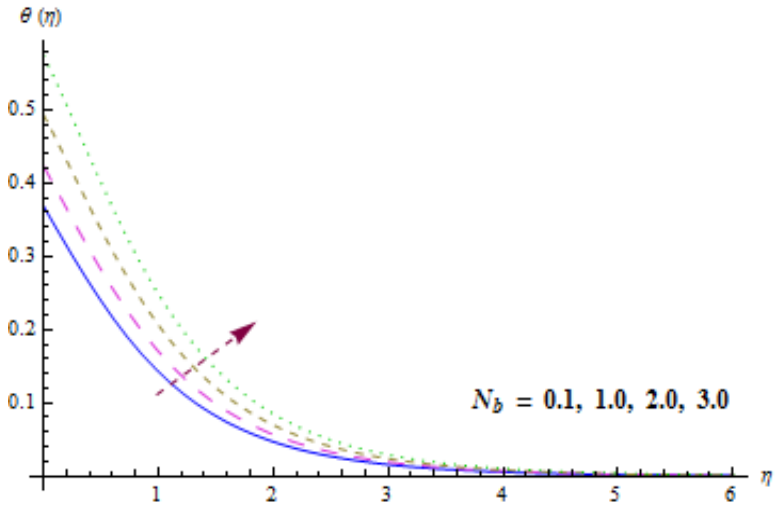

Fig. 9. $\theta(\eta)$ via variation of N_b.

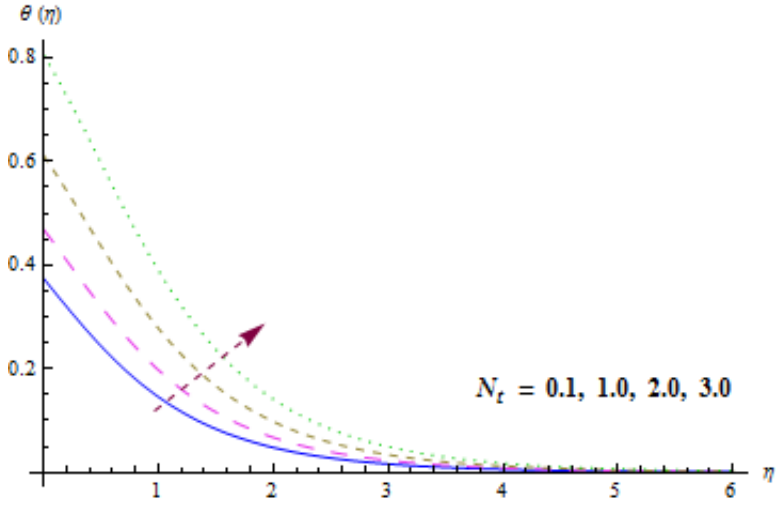

Fig. 10. $\theta(\eta)$ via variation of N_t.

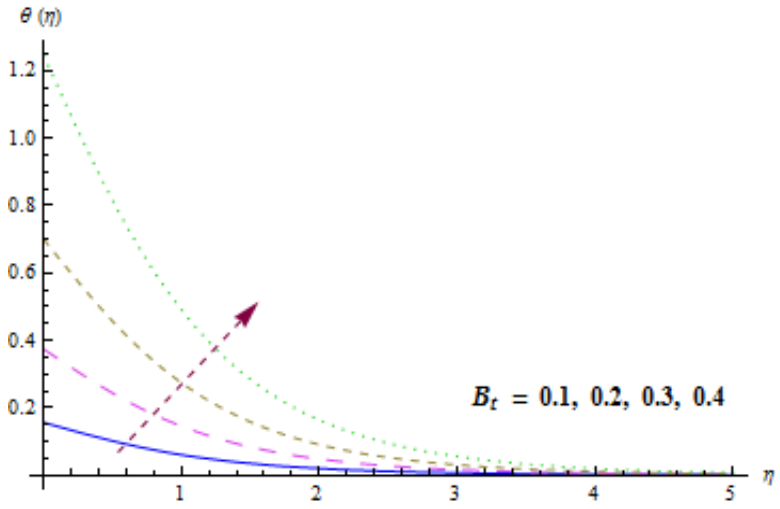

Fig. 11. $\theta(\eta)$ via variation of B_t.

4.3 Concentration field

Graphical illustration for concentration against N_b is captured in Fig. 12. One may see from the Fig. that concentration is reduced via larger N_b. In fact Brownian motion appeared in the ratio form of nanoparticle mass species equation due to which the decreasing trend is noticed. Fig. 13 witnesses that concentration field and thickness layer have increasing behavior in the frame of N_t. Explanation of Sc on concentration is demonstrated via Fig. 14. Clearly concentration and layer thickness diminishes via larger Sc. Since Sc is relation of momentum and mass diffusivities. In fact for larger Sc the mass diffusivity of the fluid decays which is responsible for reduction of concentration. Fig. 15 emphases on B_c consequence against concentration. Both concentration and layer thickness are enhanced via larger B_c.

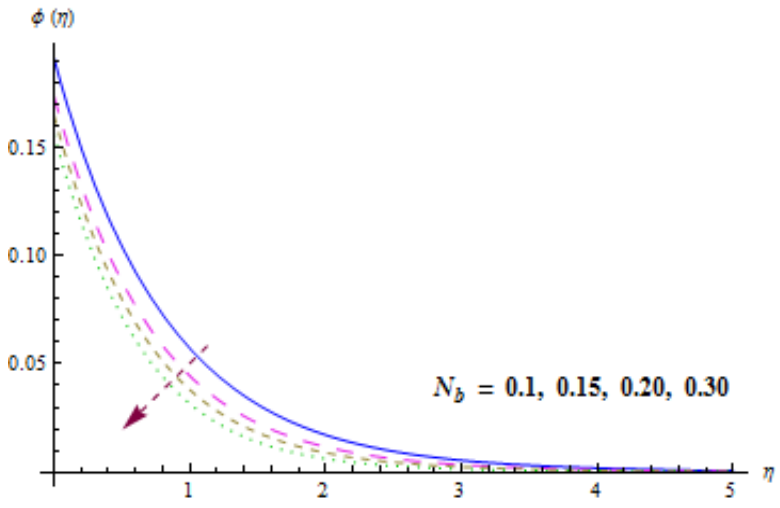

Fig. 12. $\phi(\eta)$ via variation of N_b.

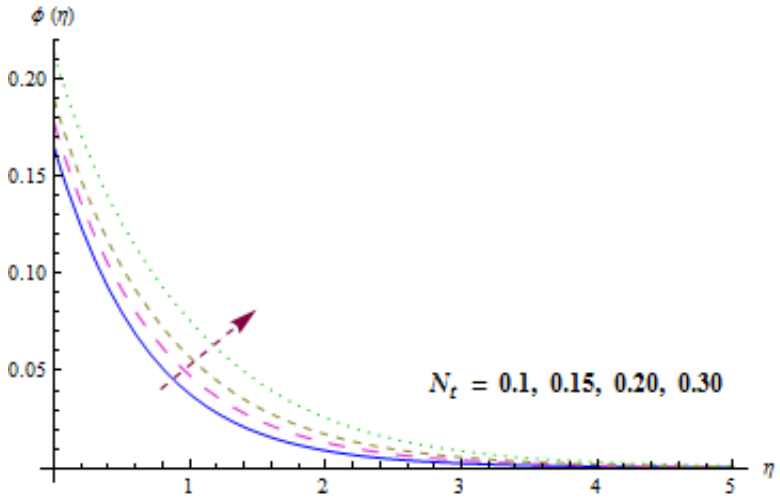

Fig. 13. $\phi(\eta)$ via variation of N_t.

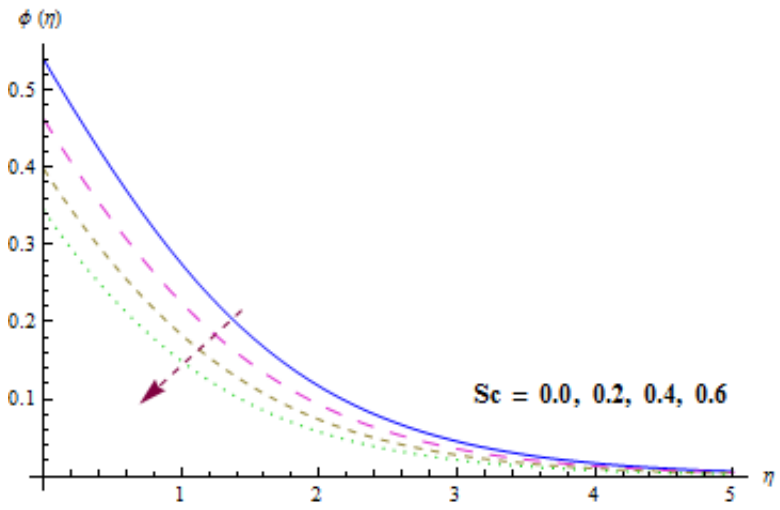

Fig. 14. $\phi(\eta)$ via variation of Sc.

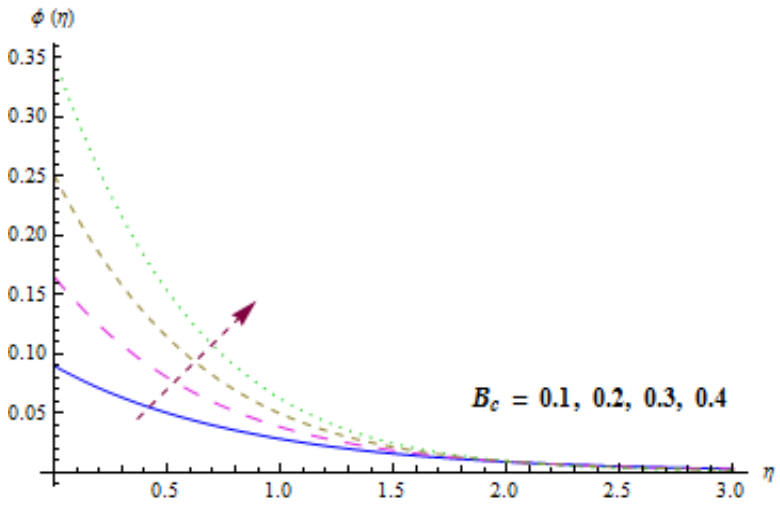

Fig. 15. $\phi(\eta)$ via variation of B_c.

4.4 Surface drag force

Features of α and H_a on surface drag force are described in Fig. 16. Here magnitude of surface drag force enhanced for larger α and H_a. Fig. 17 addresses n and λ behavior versus surface drag force. It is clear that magnitude of surface drag force are reverse for n and λ.

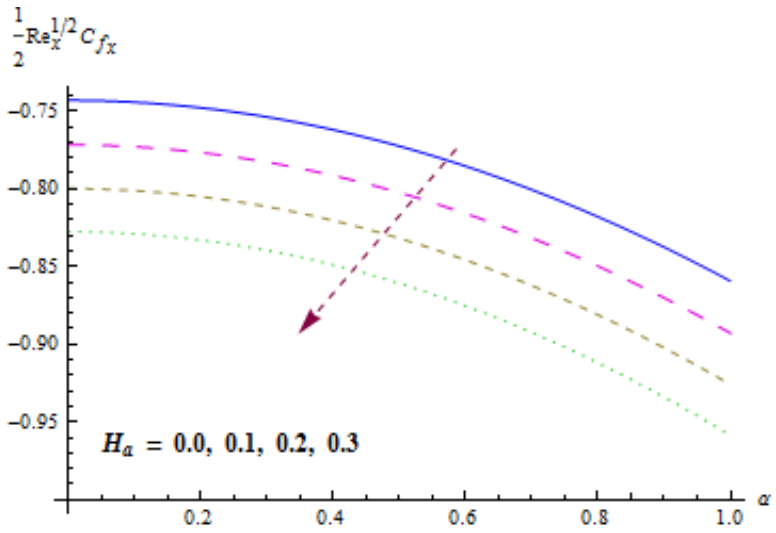

Fig. 16. $u_w(x) = ax$ via variations of α and H_a.

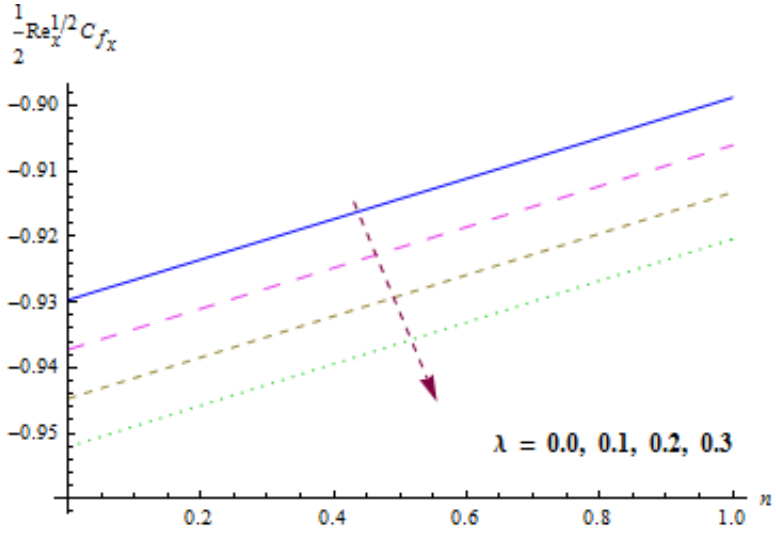

Fig. 17. $\frac{1}{2}\mathrm{Re}_x^{1/2} C_{f_x}$ via variations of n and λ.

4.5 Heat transfer rate

Fig. 18 interprets variations of heat transfer rate via B_t and Pr. Here heat transfer rate is boosted when B_t and Pr are increased. Aspects of heat transfer rate in the frame of N_b and N_t is disclosed in Fig. 19. Clearly heat transfer rate decline when N_b and N_t are increased.

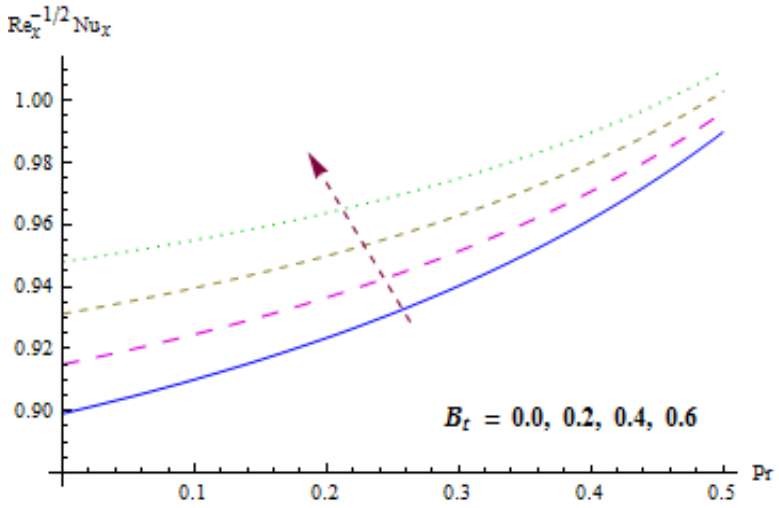

Fig. 18. $\mathrm{Re}_x^{1/2}\, Nu_x$ via variations of Pr and B_t.

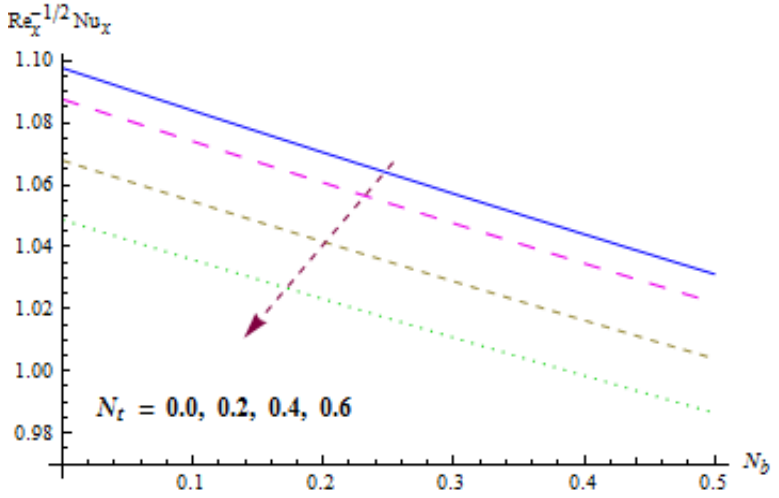

Fig. 19. $\mathrm{Re}_x^{1/2}\, Nu_x$ via variations of N_b and N_t.

4.6 Mass transfer rate

Aspects of N_b and Sc on mass transfer rate are explored in Fig. 20. It is revealed that mass transfer rate enhances via N_b and Sc. Fig. 21 provides mass transfer rate via N_t and B_c. Mass transfer rate enhances via B_c while it decay in view of N_t.

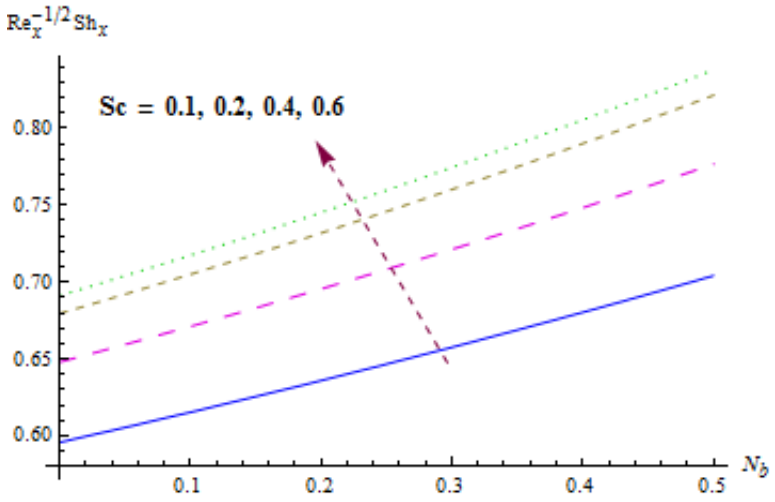

Fig. 20. $\mathrm{Re}_x^{1/2}\, Sh_x$ via variations of N_b and Sc.

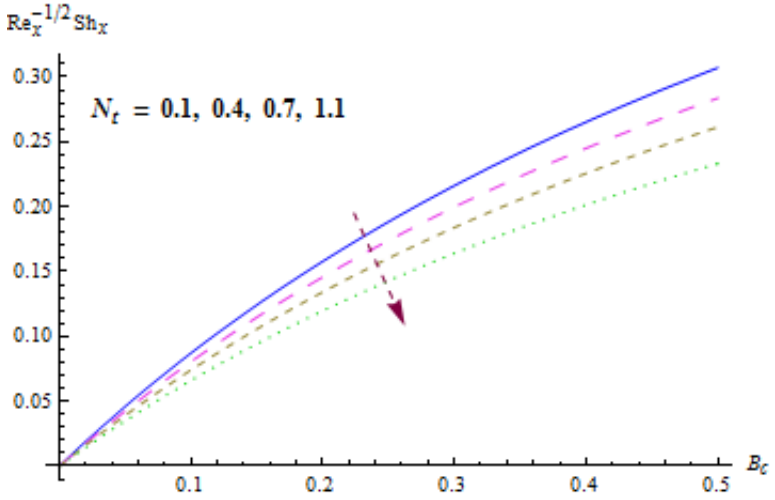

Fig. 21. $\mathrm{Re}_x^{1/2}\, Sh_x$ via variations of B_c and N_t.

Table 2: Comparison of skin friction coefficient for various values of H_a with previous exiting results when $n = 1.0,\ \alpha = 0.0,\ \lambda = 0.0,\ \beta_t = 0.0,\ N^* = 0.0$ and $\beta_c = 0.0.$

H_a	Ref. [28]	Present results
0.0	–1.00000	–1.00000
0.2	–1.01980	–1.01961
0.5	–1.11803	–1.11771
0.8	–1.28063	–1.28042
1.0	–1.41421	–1.41407

Comparative values of skin friction coefficient for the various values of H_a with previous published work are examined in Table 2. It is recognized that our results are in good agreement with the previous solutions in limiting cases.

5 Concluding remarks

The present study has following key points.

- Opposite behavior of velocity field is noticed in view of α and H_a.
- Thermal field via θ_w and B_t has similar qualitative behavior.
- Concentration and related layer thickness for N_b and N_t have reverse effect.
- Magnitude of surface drag force are reverse for n and λ.
- Heat transfer rate is boosted when B_t and Pr are increased.
- Larger Sc retards concentration while reverse scenario is noted for mass transfer rate.

References

1. Mousavi, S. M. R., et al., Analytical flow study of a conducting Maxwell fluid through a porous saturated channel at various wall boundary conditions. Eur. Phys. J. Plus, 129 (2014), pp. 181.
2. Zaib, A., et al., Dual solutions of non-Newtonian Casson fluid flow and heat transfer over an exponentially permeable shrinking sheet with viscous dissipation, Model. Simul. Eng. 2016 (2016), pp. 1-8.
3. Bird, R. B., et al., Dynamics of polymeric liquids. New York:Wiley, 1987.
4. Ali, N., Hayat, T., Peristaltic motion of a Carreau fluid in an asymmetric channel, Appl. Math. Comput. 193 (2007), pp. 535-552.

5. Hayat, T., et al., Boundary layer flow of Carreau fluid over a convectively heated stretching sheet, Appl. Math. Comput. 246 (2014), pp. 12-22.
6. Hayat, T., et al., Theoretical aspects of Brownian motion and thermophoresis on nonlinear convective flow of magneto Carreau nanofluid with Newtonian conditions, Results Phys. 10 (2018), pp. 521-528.
7. Hsiao, K. L., To promote radiation electrical MHD activation energy thermal extrusion manufacturing system efficiency by using Carreau-Nanofluid with parameters control method, Energy, 130 (2017), pp. 486-499.
8. Hayat, T., et al., Radiative flow of Carreau liquid in presence of Newtonian heating and chemical reaction, Results Phys. 7 (2017), pp. 715-722.
9. Khan, M., et al., Numerical assessment of solar energy aspects on 3D magneto-Carreau nanofluid: A revised proposed relation, Int. J. Hyd. Energy, 42 (2017), pp. 22054-22065.
10. Khan, M., et al., Impact of forced convective radiative heat and mass transfer mechanisms on 3D Carreau nanofluid: A numerical study, Eur. Phys. J. Plus, 132 (2017), pp. 517.
11. Cortell, R., Fluid flow and radiative nonlinear heat transfer over stretching sheet, J. King Saud Univ. Sci. 26 (2013), pp. 161-167.
12. Hayat, T., et al., Nonlinear thermal radiation aspects in stagnation point flow of tangent hyperbolic nanofluid with double diffusive convection, J. Mol. Liq. 223 (2016), pp. 969-978.
13. Reddy, J. V. R., et al., Impact of nonlinear radiation on 3D magnetohydrodynamic flow of methanol and kerosene based ferrofluids with temperature dependent viscosity, J. Mol. Liq. 236 (2017), pp. 93-100.
14. Soomro, F. A., et al., Melting heat transfer analysis of Sisko fluid over a moving surface with nonlinear thermal radiation via Collocation method, Int. J. Heat Mass Transf. 126 (2018), pp. 1034-1042.
15. Laxmi, T. V., Shankar, B., Effect of nonlinear thermal radiation on boundary layer flow of viscous fluid over nonlinear stretching sheet with injection/suction, J. Appl. Math. Phys. 4 (2016), pp. 307-319.
16. Hayat, T., et al., Inclined magnetic field and heat source/sink aspects in flow of nanofluid with nonlinear thermal radiation, Int. J. Heat Mass Transf. 103 (2016), pp. 99-107.
17. Makinde, O. D., Animasaun, I. L., Thermophoresis and Brownian motion effects on MHD

bioconvection of nanofluid with nonlinear thermal radiation and quartic chemical reaction past an upper horizontal surface of a paraboloid of revolution, J. Mol. Liq. 221 (2016), pp. 733-743.

18. Kumar, R., et al., Rotating frame analysis of radiating and reacting ferro-nanofluid considering Joule heating and viscous dissipation, Int. J. Heat Mass Transf. 120 (2018), pp. 540-551.
19. Qayyum, S., et al., Chemical reaction and heat generation/absorption aspects in MHD nonlinear convective flow of third grade nanofluid over a nonlinear stretching sheet with variable thickness, Results Phy. 7 (2017), pp. 2752-2761.
20. Hayat, T., et al., Modern aspects of nonlinear convection and magnetic field in flow of thixotropic nanofluid over a nonlinear stretching sheet with variable thickness, Physica B: Cond. Matt. 537 (2018), pp. 267-276.
21. Choi, S. U. S., Enhancing thermal conductivity of fluids with nanoparticle. In: Siginer, D. A., Wang, H. P. (Eds.), developments and applications of non-Newtonian flows, MD-vol. 231/FED-vol. 66. ASME, New York, (1995), pp. 99-105.
22. Buongiorno, J., Convective transport in nanofluids, J. Heat Transfer-Trans.-ASME 128 (2006), pp. 240-250.
23. Pantzali, M. N., et al., Investigating the efficacy of nanofluids as coolants in plate heat exchangers (PHE), Chem. Eng. Sci. 64 (2009), pp. 3290-3300.
24. Hamad, M. A., Pop, I., Scaling transformations for boundary layer flow near the stagnation-point on a heated permeable stretching surface in a porous medium saturated with a nanofluid and heat generation/absorption effects, Trans. Porous Medium, 87 (2010), pp. 25-39.
25. Qayyum, S., et al., Mixed convection and heat generation/absorption aspects in MHD flow of tangent-hyperbolic nanoliquid with Newtonian heat/mass transfer, Rad. Phys. Chem. 144 (2018), pp. 396-404.
26. Chakraborty, T., et al., Analytical approach to a Jeffrey nanofluid flow towards a Stagnation point coexisting with Magnetic field and Melting heat effects, J. Mol. Liq. 229 (2017), pp. 443-452.
27. Khan, M., et al., Non-linear radiative flow of three-dimensional Burgers nanofluid with new mass flux effect, Int. J. Heat Mass Transf. 101 (2016), pp. 570-576.

28. Shehzad, S. A., et al., Influence of convective heat and mass conditions in MHD flow of nanofluid, Bull. Pol. Acad. Sci. Tech. Sci. 63 (2015), DOI: 10.1515/bpasts-2015-0053.
29. Khan, M., Khan, W. A., MHD boundary layer flow of a power-law nanofluid with new mass flux condition, AIP Advances, 6 (2016), pp. 025211.
30. Khan, M., Khan, W. A., Steady flow of Burgers' nanofluid over a stretching surface with heat generation/absorption, J. Braz. Soc. Mech. Sci. Eng. 38 (2016), pp. 2359-2367.
31. Liao, S., Homotopy analysis method in nonlinear differential equations, Springer & Higher Education Press (2012).
32. Hayat, T., et al., Thermally radiative stagnation point flow of Maxwell nanofluid due to unsteady convectively heated stretched surface, J. Mol. Liq. 224 (2016), pp. 801-810.
33. Sardanyes, J., et al., Activation of effector immune cells promotes tumor stochastic extinction: A homotopy analysis approach, Appl. Math. Comput. 252 (2015), pp. 484-495.
34. Qayyum, S., et al., Effect of a chemical reaction on magnetohydrodynamic (MHD) stagnation point flow of Walters-B nanofluid with newtonian heat and mass conditions, Nuclear Eng. Tech. 49 (2017), pp. 1636-1644.
35. Liu, Q. X., et al., Asymptotic limit cycle of fractional van der Pol oscillator by homotopy analysis method and memory-free principle, Appl. Math. Model. 40 (2016), pp. 3211-3220.
36. Aquino, A. I., Bo-ot, L. Ma.T., Multivalued behavior for a two-level system using homotopy analysis method, Physica A, 443 (2016), pp. 358-371.
37. Qayyum, S., et al., Magnetohydrodynamic (MHD) nonlinear convective flow of Jeffrey nanofluid over a nonlinear stretching surface with variable thickness and chemical reaction, Int. J. Mech. Sci. 134 (2017), pp. 306-314.
38. Qayyum, S., et al., Mixed convection and heat generation/absorption aspects in MHD flow of tangent-hyperbolic nanoliquid with Newtonian heat/mass transfer, Rad. Phys. Chem. 144 (2018), pp. 396-404.
39. Qayyum, S., et al., Simultaneous effects of melting heat transfer and inclined magnetic field flow of tangent hyperbolic fluid over a nonlinear stretching surface with homogeneous-heterogeneous reactions, Int. J. Mech. Sci. 133 (2017), pp. 1-10.
40. Hayat, T., et al., Radiation effects on the mixed convection flow induced by an inclined stretching cylinder with non-uniform heat source/sink, PLoS ONE, 12 (2017), pp. e0175584.